Characterizing Plasmons in Nanoparticles and Their Assemblies with Single Particle Spectroscopy

ARTICLE *in* JOURNAL OF PHYSICAL CHEMISTRY LETTERS · JULY 2011

Impact Factor: 7.46 · DOI: 10.1021/jz200702m

3 AUTHORS, INCLUDING:

Liane Siu Slaughter
University of California, Los Angeles
18 PUBLICATIONS **1,122** CITATIONS
SEE PROFILE

Wei-Shun Chang
Rice University
49 PUBLICATIONS **2,056** CITATIONS
SEE PROFILE

THE JOURNAL OF PHYSICAL CHEMISTRY Letters

PERSPECTIVE

pubs.acs.org/JPCL

Characterizing Plasmons in Nanoparticles and Their Assemblies with Single Particle Spectroscopy

Liane Slaughter,[†,§] Wei-Shun Chang,[†,§] and Stephan Link[†,§,‡,*]

[†]Department of Chemistry, [‡]Department of Electrical and Computer Engineering, and [§]Laboratory for Nanophotonics, Rice University, Houston, Texas, United States

ABSTRACT: The plasmonic properties of noble-metal nanoparticles are extremely sensitive to their size and shape. Single particle spectroscopy techniques have therefore become the standard for understanding how the energy of the localized surface plasmon of individual nanoparticles scales with small changes in the morphology. Chemical methods have progressed to the point where researchers can facilely grow and assemble plasmonic nanostructures potentially useful for improving technologies in computing, communication, biomedical imaging and sensing, and therapeutics. Very small and very large nanostructures each present a unique set of challenges, and a separate strategy for each kind of sample is necessary for fully revealing the relationships among size, shape, orientation, and spacing between nanoparticles. This Perspective discusses how different single particle imaging and spectroscopy techniques together with electron microscopy can be applied to reveal the relationships between the plasmonic response and the morphology of individual nanoparticles as well as their assemblies. In particular, we show examples from our own studies that examined large nanostructures and disordered assemblies.

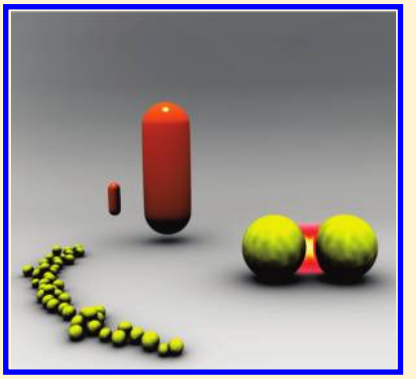

The surface plasmon resonance (SPR), a coherent oscillation of the conduction band electrons, imparts striking and rich properties to noble metal nanoparticles (NPs).[1−3] The resonance frequency of the SPR is strongly affected by changes in the size, shape, and surrounding environment of the NP. The SPR causes the NP to have extremely high absorption and scattering cross sections compared with molecular dyes. Gold NPs are biologically inert while having easily accessible surface chemistry and an SPR that can be tuned from the visible to the infrared regions and have therefore already provided favorable nanostructured platforms for contrast markers, drug and gene delivery vehicles, and cancer therapy agents.[4−12] The sensitivity of the SPR to the size and shape of the NP does, however, lead to a distribution of optical properties within the same sample of NPs, especially if they are grown in solution. Because the SPR wavelength must be tuned within a spectral window to optimize their efficiency for certain applications, single particle spectroscopy techniques have emerged as an important tool for unraveling the detailed relationships between the geometry and the SPR of the NPs.[13,14]

The SPR is furthermore affected by its environment, not only through the refractive index of the surrounding medium but also by the presence of other NPs. The SPRs of closely spaced NPs, often assembled from the bottom-up to achieve the smallest gaps, can delocalize over multiple NPs.[5,15−25] The strength of the interaction is governed by the interparticle distance and can be understood analogously to molecular bonding using plasmon hybridization theory.[16,20,23,24,26] The large enhancements of the electric field between NPs coupled in the near-field have been explored thoroughly for surface-enhanced spectroscopies.[1,7,27−32] More recently, researchers have developed elegant strategies to use these interactions between gold and silver NPs to measure molecular distances and forces.[5,25,33] The interactions between small numbers of NPs can be addressed comprehensively with combinations of single particle techniques and computations.[15,18,22,23,34−36] For chemically prepared and assembled NPs, the majority of such combined experimental and theoretical studies have, however, addressed only small assemblies with typically <5 NPs.[18,22,23] Plasmon interactions in larger assemblies nonetheless have significant implications for receiving, transmitting, and propagating optical signals in nanostructures smaller than the diffraction limit of light.[37−41]

Many recent advances in controlling and understanding the surface chemistry of gold NPs of various shapes lend tremendous promise to facilely forming highly tunable and functional assemblies both on substrates and in solution.[42−48] Constructing these assemblies from the bottom-up with NP building blocks allows closer spacings than those typically achieved by top-down fabrication methods but also imparts more irregularities.[42,44−46] Realizing the full potential of these structures therefore requires identifying and characterizing the nature of plasmon coupling among the NPs and the role of defects. Correlated structural imaging using electron microscopy combined with single particle spectroscopy has significantly advanced our initial understanding of complex assembled nanostructures consisting of plasmonic NPs.[18,19,34,35] This Perspective addresses considerations and challenges unique to single particle spectroscopy of NPs having

Received: May 24, 2011
Accepted: July 22, 2011
Published: July 22, 2011

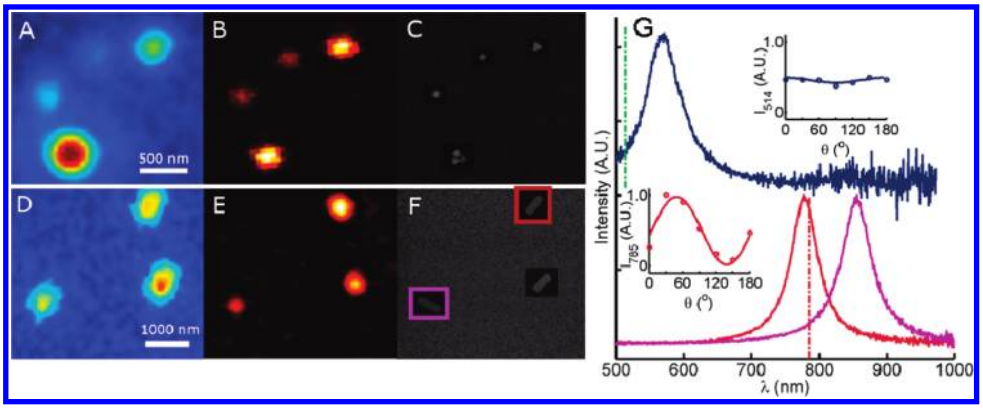

Figure 1. Correlated DF scattering (A,D), photothermal absorption (B,E), and SEM (C,F) images of 40 nm gold nanospheres (top row) and gold nanorods with mean dimensions of 22 × 70 nm (bottom row). Parts C and F feature higher magnification SEM images cropped onto a lower magnification image to illustrate simultaneously the morphology and locations of the NPs. Parts A−C and D−F are not scaled to each other. (G) DF scattering spectra of a single gold nanosphere (top) and two gold nanorods (bottom) corresponding to the brightest (28 × 77 nm, maroon) and dimmest (85 × 27 nm, violet) spots seen in part E. The dotted green and red lines indicate wavelengths of 514 and 785 nm used for exciting the NPs in parts B and E, respectively. The insets show the polarization dependence of the absorption intensity measured using 514 nm for the nanosphere (top) and 785 nm for the brightest nanorod (bottom).

different shapes and falling into different size regimes as well as assemblies supporting various extents of interparticle interactions. In particular, we have ventured into the realm of highly varied and irregular large-scale quasi 1-D assemblies, revealing some unique characteristics of the nature of plasmon coupling in these structures.

Determining the size and shape accurately through high-resolution scanning and transmission electron microscopy (SEM and TEM) is critical to understanding the strong dependence of the SPR on the morphology of the NP. Single particle spectroscopy, in combination with these electron microscopy techniques, enables one to determine how subtle differences in size, shape, orientation, and arrangements of NPs affect their absorption and scattering properties. Sample preparation must therefore allow one to "map" the exact location of a unique nanostructure in multiple electron and optical microscopes. Specifically, single NPs and small aggregates can be pinpointed in both electron and optical microscopes if they are dispersed on a patterned substrate at low concentration. Dozens of researchers have employed simple and convenient ways to map NPs between multiple microscopic imaging schemes at high and low magnifications.[27,29,49−51] Figure 1 demonstrates an example where we recorded scattering (A,D) and absorption (B,E) images of individual gold NPs and their scattering spectra (G) and separately located the exact same NPs by SEM (C,F). Dark-field (DF) scattering and photothermal heterodyne imaging (PHI) were used as background-free techniques for measuring either only scattering or absorption of spherical (A,B) and rod-shaped (D,E) NPs.[13,23,52−56] DF scattering relies on collecting the scattering of NPs at a smaller angle than the incident light and is straightforward to employ for NPs >20 nm.[57] PHI, first reported 10 years ago, is a powerful and sensitive technique for imaging single plasmonic NPs with diameters as small as 1.4 nm.[53,58,59] Direct single particle absorption measurements are nontrivial compared with DF scattering measurements, given that absorption usually measures small changes of a much larger incident radiation, but PHI circumvents this issue by probing changes in the refractive index of the medium surrounding the NP due to NP heating caused by absorption.[53]

Comparing Figures 1A and 1C, this DF image provides strong contrast among the two single 40 nm gold NPs, one triangular NP, and the aggregate that consists of NPs that are separated by a distance smaller than the resolution of the microscope. However, an analysis of the DF scattering image (Figure 1A) based on intensity values alone can be misleading and is especially dangerous without the correlated SEM image (Figure 1C). Because the absorption and scattering of plasmonic NPs does not show intensity fluctuations ("blinking") as seen for single dye molecules,[5,60] the most reliable method to identify single NPs and distinguish them from small aggregates that cannot be optically resolved is to employ correlated electron microscopy. Compared with the scattering image (Figure 1A), the absorption image (Figure 1B), obtained with 514 nm laser excitation, shows that PHI unambiguously detects the single NPs against a reduced background. This difference is due to the different scaling of absorption and scattering with NP volume, V (absorption scales as V, whereas scattering scales as V^2 for NPs smaller than ~100 nm[56,61]), and can be applied here as a first approximation. The fact that the PHI images are recorded with a fixed wavelength instead of integrated over the entire spectrum can lead to smaller contrast between a single NP and an aggregate, depending on the resonance wavelength of the NP and considering that coupled SPR modes are red-shifted from the single NP resonance. (See below for more discussion of dimers.)

An analysis of the DF scattering image based on intensity values alone can be misleading and is especially dangerous without the correlated SEM image.

Single particle spectra provide the quantitative information necessary for evaluating the dependence of the SPR on the

dx.doi.org/10.1021/jz200702m | J. Phys. Chem. Lett. 2011, 2, 2015–2023

geometries of the NPs. Representative single particle spectra from the nanosphere and nanorod samples are displayed in Figure 1G. The longitudinal SPR of the nanorods at 775 and 860 nm are easily differentiated from the SPR of the 40 nm nanospheres at 570 nm. In addition to the large spectral shift of the SPR, when changing the shape from a sphere to a rod, small variations in the nanorod aspect ratio, even for nanorods from the same sample, lead to significant differences in the maximum of the longitudinal SPR, causing inhomogenous broadening of the SPR line width in ensemble measurements.[62] For the PHI measurement of rods in Figure 1E, acquired with excitation at 785 nm, this distribution in SPR maxima results in a larger intensity distribution compared with the DF scattering image in Figure 1D. The mean dimensions of the nanorod sample are 70 × 22 nm, but the spectra in Figure 1G correspond to rods that are 77 × 28 nm (maroon) and 85 × 27 nm (violet), yielding the brightest and dimmest spots in Figure 1E, respectively. The spectral positions of the SPR peaks relative to the excitation wavelength (dotted red line) directly account for these differences in intensity.

A nanorod is further distinguished from an isotropically shaped NP through polarization-dependent absorption measurements in addition to the more common DF scattering experiments.[14,55,63] The inset in the bottom part of Figure 1G shows that one can selectively detect the longitudinal surface plasmon absorption of the nanorod in the PHI method by choosing the appropriate wavelength of the excitation light and changing its polarization, θ. The polarization-dependent PHI intensity can be described by $I(\theta) = N(1 + M \cos 2(\theta - \phi))$, where M is the modulation depth, ϕ is the orientation of the nanorod's long axis, and N is a normalization factor.[54] M for the nanorod excited at 785 nm is nearly 1, indicating very strong polarization anisotropy compared with exciting a 40 nm NP near its SPR wavelength with 514 nm (inset in the upper part of Figure 1G).

Whereas the longitudinal SPR yields maximum polarization anisotropy when the excitation wavelength is tuned to the resonance, we have also shown that with the appropriate choice of the optical geometry one can achieve sufficient modulation depth from the transverse mode excited at 514 nm to determine the nanorod's orientation.[54] The transverse SPR is less sensitive to changes in the size of the nanorod and its dielectric environment than the longitudinal SPR.[3,64] Therefore, this approach overcomes the difficulties of relying on the longitudinal SPR, which can significantly affect the measured signal for a distribution of nanorod aspect ratios, as already shown in Figure 1E. DF scattering and PHI are therefore complementary imaging techniques, which, when combined with electron microscopy, provide a powerful set of tools for correlating optical spectra with the morphology of the NPs.

NPs falling into different size regimes present unique challenges for the optical schemes designed to characterize them. Figure 1 already illustrates the difficulty of distinguishing small individual NPs from clusters of a few NPs by optical microscopy alone. Larger NPs with diameters d > 100 nm have much larger cross sections and are therefore easier to observe, but their spectra are more complex and show multiple SPR bands, which furthermore quickly red-shift beyond the detection window of common CCD detectors.[52,62] Figure 2 compares two nanorods of the same aspect ratio but with very different sizes: 120 × 370 nm compared with 24 × 74 nm. For fully characterizing the larger nanorod, we developed another strategy that allowed us to

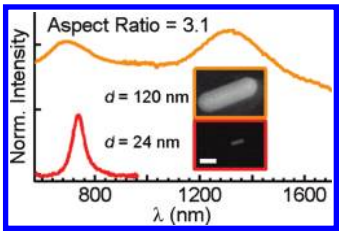

Figure 2. Single particle extinction spectrum (top, orange) of a 120 × 370 nm gold nanorod and DF scattering (bottom, red) of a smaller rod having the same aspect ratio, with dimensions 24 × 74 nm. The corresponding SEM images are shown as insets. The scale bar represents 100 nm. Reprinted from ref 52.

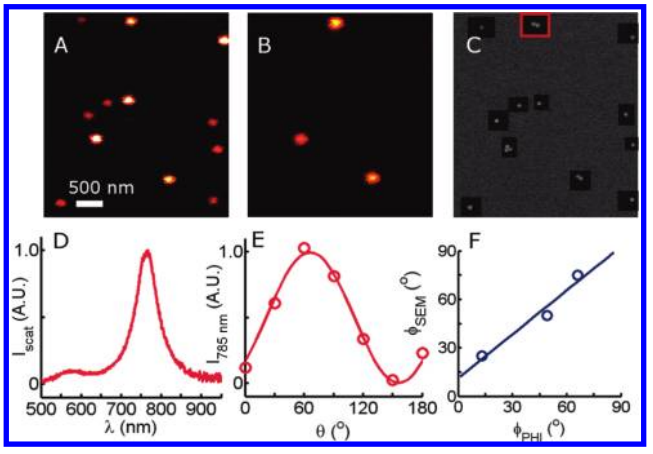

Figure 3. Photothermal images of individual 40 nm gold nanospheres and multimers excited with 514 nm laser light (A) and 785 nm laser light (B). (C) SEM images at high magnification (50 000×), showing whether they are single NPs, arranged on a lower magnification image (15 000×) showing their location in the area imaged in parts A and B. (D) DF scattering spectrum of the dimer boxed in part C. (E) Dependence of the photothermal intensity of the same dimer excited at 785 nm on the polarization of the excitation light. The angle, θ, is measured relative to a vertical line in the counter-clockwise direction. (F) Comparison of the orientations of three dimers identified in SEM to their orientations measured by polarization-dependent photothermal excitation at 785 nm.

record single particle spectra of larger NPs with SPRs beyond 1000 nm. The spectrum (top, orange) of the larger 120 × 370 nm gold nanorod was acquired through ultra broad-band extinction spectroscopy, whereas that of the smaller 24 × 74 nm nanorod (bottom, red) was measured by DF scattering spectroscopy, as described above.[52] For the extinction spectrum, a transmission geometry was employed that combined a Si CCD detector, for wavelengths from 500 to 1000 nm, with an InGaAs single array detector, which allowed us to acquire the signal in the range of 1000−2000 nm. Because of the large SPR cross section, no spatial modulation was necessary to enhance the signal.[65] The larger nanorod with d = 120 nm exhibits a dipole SPR peak near 1350 nm, a red shift of >500 nm compared with the dipole mode of the smaller nanorod with d = 24 nm. For nanorods with d < 30 nm, the quasi-static approximation can be applied[66] and the maximum of the longitudinal dipole mode scales linearly with the aspect ratio. Outside this size regime, however, retardation and dynamic depolarization lead to inhomogeneities of the electric field across the NP.[52,62,66−71] These effects cause red-shifting of

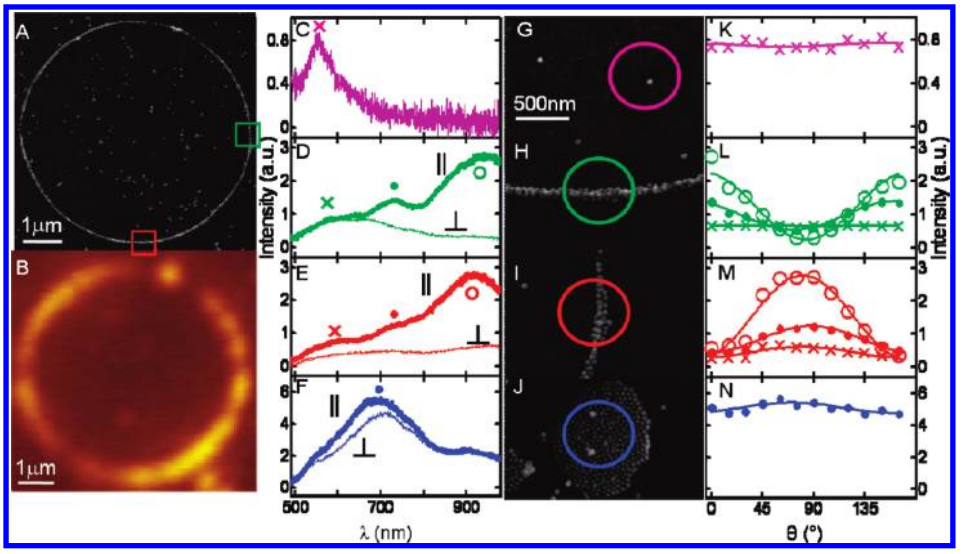

Figure 4. SEM (A) and the corresponding DF scattering image (B) of a ring with a diameter 6.6 μm composed of 40 nm gold NPs functionalized with polystyrene. DF scattering spectra of a single gold NP (C), the two ring segments (D,E) highlighted in part A, and an NP aggregate (F). The thick and thin lines show spectra recorded for scattered light polarized parallel and perpendicular to the major axis of the NP assembly, respectively. The corresponding SEM images are given in the middle column. The size of the detection area is highlighted by the colored circle. (H,I) Magnified views of the ring segments marked by the rectangles in part A. (K,N) Polarization dependence of the plasmon resonances of the single particle and the aggregate in parts C and F, respectively. (L,M) Polarization dependences of the three different maxima of the two ring segments. The intensity scale on the right matches the one on the left. Reprinted from ref 19.

the dipole SPR peak as the absolute dimensions increase and the presence of higher order SPR modes at higher energies, even when the aspect ratio is maintained.[52,62,69−72] Higher order longitudinal modes are part of the broad band peaked at 690 nm, as revealed by polarized spectra.[52]

Correlated single particle spectroscopy techniques and electron microscopy are particularly necessary for studying how arranging NPs relative to each other affects the optical properties of the assembly compared with isolated NPs. Figure 1 already showed results obtained by single particle microscopy on closely spaced assemblies of NPs. In Figure 3, we take a closer look at dimers of 40 nm gold NPs, which exhibit behavior analogous to that of individual anisotropically shaped nanostructures. The photothermal images in Figure 3A,B and the corresponding SEM image in Figure 3C demonstrate the relationship between the photothermal intensity for a specific wavelength and the SPR of the individual NPs and multimers (dimers and trimers). Scattering spectroscopy reveals that the SPR maximum of the dimer (3D) is red-shifted more than 200 to 765 nm compared with the SPR of the individual NP (Figure 1G). This shift can be explained by the bonding interaction of parallelly orientated dipoles within the framework of plasmon hybridization theory, which analytically provides the energies of the coupled modes for assemblies of small NPs as well as an intuitive picture of plasmon interactions.[16] The antibonding dimer mode, in contrast, is only weakly coupled and is slightly blue-shifted with respect to the single NP SPR.[16] Therefore, individual and multimers of 40 nm gold NPs absorb at 514 nm (Figure 3A), but only dimers and trimers of these NPs absorb at 785 nm (Figure 3A). Whereas circularly polarized excitation was used to acquire the images in Figure 3A,B, the PHI intensity of the dimer excited at 785 nm with linearly polarized laser light shows a similar polarization dependence (Figure 3E) as the PHI intensity of the nanorod (Figure 1G); the maximum intensity is recorded when the polarization is parallel to the longitudinal dimer axis. Similar to the behavior of the nanorod (inset in Figure 1G), the polarization dependence of the dimer shown in Figure 3E can be fit with $I(\theta) = N(1 + M \cos 2(\theta - \phi))$, again yielding $M \approx 1$. The red-shifted SPR peak and its sensitivity to polarization liken the dimer to a nanorod and suggest that they too can be used as orientation sensors while simultaneously serving as rulers of small distances.[5] Figure 3F compares the orientations of three dimers visualized by SEM with their orientations derived by polarization-sensitive PHI with 785 nm laser excitation, which clearly shows that dimer orientations can be accurately determined by optical methods.[25]

Considering the ensuing discussion, we cannot necessarily exclude that the NPs in the multimers in Figure 3 were not touching. The spectrum in Figure 3D, however, is consistent with a small gap in between the NPs in this dimer. In addition, DF spectra were taken before and after PHI measurements to confirm that no laser induced melting occurred.

Figures 1−3 illustrate how we can choose different combinations of single particle spectroscopy techniques to characterize thoroughly a variety of NPs of different sizes and shapes as well as small NP assemblies such as dimers. Interactions within larger and more irregular assemblies are difficult to unravel rigorously compared with isolated structures and small assemblies. Strategies drawn from the same pool of single particle techniques nonetheless attest to the ability of such structures to support highly coupled collective plasmon modes.[19,73,74] Polarization-sensitive single particle studies on local areas of micrometer diameter rings self-assembled from 40 nm gold NPs revealed collective low-energy plasmon modes polarized parallel to the local alignment of the ring that seemed tolerant of irregularities in the NP arrangement.[19]

Interactions within larger and more irregular assemblies are difficult to unravel rigorously compared with isolated structures and small assemblies.

An NP ring with a diameter of 6.6 μm was imaged using SEM (Figure 4A) and DF scattering (Figure 4B). A pinhole was placed at an intermediate image plane to isolate scattering from only the areas circled in Figures 4G−J. The spectra of the ring sections in Figure 4D,E show multiple plasmon modes that are red-shifted from the SPR maximum of the constituent NPs (Figure 4C). These collective plasmon modes are furthermore highly polarized along the axis of the assembly, striking evidence of strong near-field plasmon coupling. In contrast with the scattering spectrum of the dimer (Figure 3D), the spectra in Figure 4D,E comprise more plasmon modes, which indicate that nearest neighbor interactions, although strongest, do not solely account for the spectra. The maximum extent of the interactions in the "transverse" ring modes shown in the perpendicularly polarized spectra (Figure 4D,E) is limited to the width of the ring segments, two to three NPs as illustrated in the corresponding SEM images (Figure 4H,I). Given the absence of red-shifted collective plasmon modes in the perpendicularly polarized spectra, the longitudinal interactions along the quasi 1-D assembly therefore most likely occur over many more NPs. In some regions, we cannot discern whether the particles are touching, whereas other segments show clear separations between adjacent NPs. Despite these irregularities in the local geometric arrangements of the NPs, spectra taken from different segments along the same and different rings share similar features. These similarities further support plasmon coupling over many NPs. Averaging over several local ring segments within the detection area could also contribute to the observed similarity between ring spectra but is not expected to be the dominant factor.

Similar to the comparison between NP dimers and nanorods, the results in Figure 4 raise the question of whether the collective plasmon modes in a larger quasi 1-D assembly of NPs behave in parallel with the longitudinal plasmon modes of continuous metallic nanorods or nanowires. The peaks in the spectra of the ring segments are indeed more red-shifted and more sensitive to polarization than the modes observed for the 2-D aggregate shown in Figure 4J, again highlighting the influence of the assembly's aspect ratio. We previously compared the coupled modes with empirically derived scaling laws for multipoles of long nanorods.[75] This qualitative comparison suggested that the collective mode is delocalized over ~10 NPs, consistent with simulations of linear NP chains.

Because the spectra of local ring segments extend beyond the spectral window of the Si CCD camera and for comparison with the 120 × 370 nm nanorod in Figure 2, we acquired the IR extinction spectrum for the NP ring segment shown in Figure 5. Note that the width of the NP ring is approximately equal to the diameter of the rod. The polarized extinction spectrum in Figure 5 shows several more peaks beyond 1000 nm and indicates that all coupled plasmon modes beyond 700 nm have

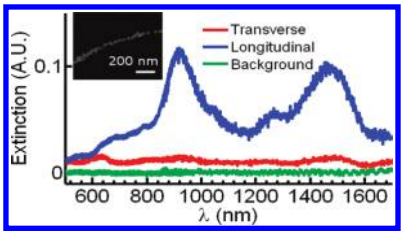

Figure 5. Longitudinally (blue) and transversely (red) polarized vis-IR extinction spectra of the ring segment shown in the SEM image. The ring was composed of 40 nm gold NPs and had a diameter of 4.1 μm. The spectrum of the glass background is shown in green.

primarily longitudinal polarization. The spectrum in Figure 5 is clearly more complex than that of the broad rod in Figure 2, but there are some qualitative similarities nonetheless. The transversely polarized scattering spectrum of both the rod and the ring segment show a broad peak centered between 600 and 700 nm. For longitudinal polarization, the dipole SPR of the broad rod and the longest wavelength peak of the ring segment are located between 1300 and 1500 nm.

The extent of the red shift for the lowest energy coupled mode in the NP ring compared with the single NP SPR is rather surprising. Theoretical studies of ordered linear chains as a function of the number of NPs have predicted that the red shift saturates for the coupled longitudinal dipole mode.[21,39,40] The infinite chain limit is typically reached for chains with 10 NPs. Our own calculations using generalized Mie theory revealed that it is not possible to push the longest wavelength SPR in linear chains of up to 50 40 nm gold NPs with 1 nm gaps beyond 1000 nm (unpublished results). Introducing defects and curvature to model the experimental NP arrangement in an NP ring segment led to only blue shifts of the coupled dipole SPR. The most likely explanation for the lowest energy SPR is therefore the conductive interaction between nearly touching NPs. In this interaction regime, conduction of electrons between NPs creates charge transfer plasmons with even further red-shifted modes that are not possible when the NPs are only capacitively coupled.[23,25,76] The presence of touching NPs in the local ring segments also explains the qualitative similarity to the broad rod. Although qualitative comparisons can give important insight into plasmon coupling in larger NP assemblies, it is apparent that the spectra of these ring segments are more complex than the spectrum of a perfectly ordered linear chain or a continuous nanorod, highlighting the fact that assemblies of NPs studied experimentally are inherently more difficult to understand than regular assemblies or continuous structures. Importantly, the latter can also be solved more easily using computational methods. Whereas it is a challenging task to separate capacitive and conductive plasmon interactions in the NP ring, we can at least investigate it at the level of a dimer, the simplest kind of assembly, as discussed next.

A study of gold nanorod dimers using DF scattering gave important insight into the allowed plasmon modes for capacitive and conductive coupling.[23] Figure 6 shows the unpolarized DF scattering spectra of dimers formed from chemically prepared gold nanorods. The bottom spectrum (red) is the scattering from a dimer, which consists of gold nanorods with dimensions of 80 × 29 nm (left rod) and 74 × 32 nm (right rod) and aspect ratios of 2.8 and 2.3, respectively. Simulations of a perfectly symmetric nanorod dimer aligned end-to-end predict a single

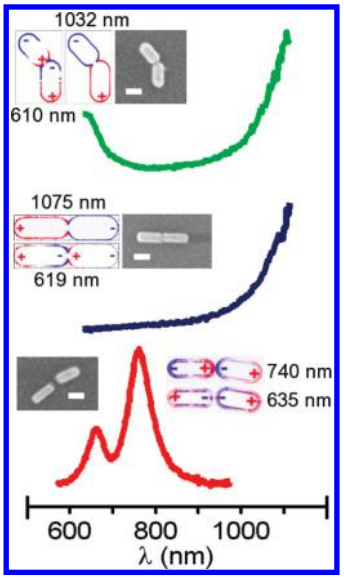

Figure 6. Unpolarized DF scattering spectra and corresponding SEM images of dimers of gold nanorods with varying asymmetry factors and extent of metallic contact: bent with metallic contact (top, green), linear with metallic contact (middle, blue), and a slightly off-linear heterodimer with no contact (bottom, red). The scale bars represent 50 nm. The charge plots were calculated for spectral features identified in FDTD simulations of the same dimers. Reprinted from ref 23.

SPR peak that is red-shifted from that of the individual nanorods and is designated as the dipole bonding mode within the concept of plasmon hybridization theory.[16,20,23,26] Our experiments, in combination with finite difference time domain (FDTD) simulations and plasmon hybridization theory, have shown that the shorter wavelength peak in Figure 6 results from antibonding interactions.[23] The antibonding dimer mode, which is blue-shifted from the SPRs of the individual nanorods having the same size as those comprising the dimer, has a nonzero dipole moment because of the asymmetry in size and shape of the two nanorods. The charge distributions of the bonding and antibonding plasmon modes are given in the inset of Figure 6, illustrating the parallel and antiparallel alignment of the dipoles. These results highlight the influences of small variations in size, shape, and spatial arrangement on plasmon coupling in small isolated NP assemblies.

Conductive contact between the NPs gives rise to new plasmon modes, which are not possible when the NPs are separated.[17,23,65,76] The middle spectrum in Figure 6 (blue) shows an SPR peak that is drastically red-shifted beyond 1100 nm and cannot be fully resolved by our Si CCD camera.[23] For this nanorod dimer, we cannot discern by SEM whether these nanorods are touching, but we infer from the scattering spectrum and FDTD simulations that the observed peak is due to a mode that occurs only through conductive interaction.[23] The charge density plot shows that the conductive mode resembles the dipole mode of a continuous nanorod having twice the length of the constituent nanorods. The charge distribution, which previously corresponded to the bonding dipole mode, is now blue-shifted and resembles the octopole of an extended nanorod. This mode is weak for the linear touching dimer but gains intensity for a bent dimer with conductive contact (top spectrum (green) of Figure 6), again demonstrating the effect of reducing the degrees of symmetry for a NP dimer. Note that the nanorod dimers are too small to have a large enough cross section for the type of extinction measurements shown in Figures 2 and 5.

For NPs <1 nm apart, the interaction between conduction electrons of neighboring NPs transitions from a capacitative interaction, that is, dominated by electromagnetic attraction and repulsion, to a conductive interaction, where electrons can tunnel between the NPs, even if they are not yet touching.[15,65,76,77] Conductive contact allows new plasmon modes of the assembly to arise that do not exist in the noncontact regime. Quantum mechanical electron tunneling and nonlocal effects of the dielectric function in the intermediate distance range between capacitive and conductive coupling also play a role and are actively investigated.[61,76] The extent of red-shifting that occurs due to conductive contact between two NPs suggests that conductive interactions are likely to also contribute to the red-shifted plasmon modes observed in the spectra of the self-assembled rings. Figure 6 therefore affirms that we must consider conductive interactions to explain the coupled plasmon modes of the NP ring shown in Figures 4 and 5. Although the polymer coating on the NPs forming the rings is expected to keep the NPs 2 to 3 nm apart,[46] conductive contact can still occur at localized points, especially if the coating is uneven and considering that the molecules on the NP surface can rearrange. These issues are especially relevant to those specializing in correlated single particle spectroscopy and electron microscopy when one cannot discern by SEM whether the NPs are touching each other. Whereas correlating high-resolution TEM images with DF scattering, extinction, or Raman spectroscopy is possible,[27,29,78] even high-resolution TEM yields only a 2-D projection of 3-D objects, thereby obscuring important topographical and structural details. Lack of such structural information together with conductive coupling and nonlocal effects at short interparticle distances as well as a large number of NPs in an assembly remain significant challenges for matching simulations to experiments.

Lack of such structural information together with conductive coupling and nonlocal effects at short interparticle distances as well as a large number of NPs in an assembly remain significant challenges for matching simulations to experiments.

Nanorod dimers and single NPs can be understood well through a combination of electron microscopy, optical spectroscopy, and simulations. Expanding such a strategy to larger assemblies of chemically prepared NPs, however, can be nontrivial. Remarkable progress in single particle spectroscopy techniques has allowed researchers to characterize the plasmonic properties of nanostructures more thoroughly than before, but achieving a quantitative understanding of the interactions among plasmonic NPs requires more work given the extent of coupling,

delocalization, and contributions from conductive and nonconductive interactions as well as nonlocal effects in larger NP assemblies, such as the ring superstructures. We have therefore expanded our studies to linear NP chains with small interparticle spacings while controlling the widths and lengths of the overall assembly to investigate in detail the evolution of coupled plasmon modes from a few NPs to tens and hundreds of NPs.

AUTHOR INFORMATION

Corresponding Author
*E-mail: slink@rice.edu.

BIOGRAPHIES

Liane Slaughter is a Ph.D. candidate in chemistry with Stephan Link at Rice University. She received her B.A. in chemistry from Cornell University (2007). Her research interests include self-assembly and the properties of self-assembled nanoparticles.

Wei-Shun Chang is a postdoctoral researcher with Stephan Link in the Department of Chemistry at Rice University. He received his Ph.D. from UT Austin (2007) with Paul Barbara. His current research interests are the radiative and nonradiative properties of strongly coupled plasmons in nanoparticle assemblies.

Stephan Link is an assistant professor in the Departments of Chemistry and Electrical and Computer Engineering at Rice University. He received his Ph.D. from Georgia Tech (2000) working with Mostafa El-Sayed. The main interest of his research group is the study of the optical properties of plasmonic nanomaterials (http://www.owlnet.rice.edu/~slink/).

ACKNOWLEDGMENT

This work was funded by the Robert A. Welch Foundation (C-1664), the National Science Foundation (CHE-0955286), and a 3M nontenured faculty grant. We would like to thank all coauthors and collaborators: Dr. Eugene Zubarev, Dr. Bishnu Khanal, Dr. Prammit Manna, Dr. Peter Nordlander, Dr. Yanpeng Wu, Dr. Alexei Tcherniak, Britain Willingham, Pattanawit Swanglap, Ji Won Ha, Sergio Dominguez-Medina, David Solis, and Saumyakanti Khatua. We would also like to thank Dr. Christy Landes and her research group, Dr. James Tour, Dr. Jason Hafner, Dr. Naomi Halas, Dr. Bruce Johnson, and Dr. Bruce Weisman for fruitful discussions and use of their equipment.

REFERENCES

(1) Landes, C. F.; Link, S.; Mohamed, M. B.; Nikoobakht, B.; El-Sayed, M. A. Some Properties of Spherical and Rod-Shaped Semiconductor and Metal Nanocrystals. *Pure Appl. Chem.* **2002**, *74* 1675–1692.

(2) Tao, A. R.; Habas, S.; Yang, P. Shape Control of Colloidal Metal Nanocrystals. *Small* **2008**, *4*, 310–325.

(3) Link, S.; El-Sayed, M. A. Shape and Size Dependence of Radiative, Non-Radiative and Photothermal Properties of Gold Nanocrystals. *Int. Rev. Phys. Chem.* **2000**, *19*, 409–453.

(4) Baciu, C. L.; Becker, J.; Janshoff, A.; Sonnichsen, C. Protein-Membrane Interaction Probed by Single Plasmonic Nanoparticles. *Nano Lett.* **2008**, *8*, 1724–1728.

(5) Sonnichsen, C.; Reinhard, B. M.; Liphardt, J.; Alivisatos, A. P. A Molecular Ruler Based on Plasmon Coupling of Single Gold and Silver Nanoparticles. *Nat. Biotechnol.* **2005**, *23*, 741–745.

(6) Huschka, R.; Neumann, O.; Barhoumi, A.; Halas, N. J. Visualizing Light-Triggered Release of Molecules inside Living Cells. *Nano Lett.* **2010**, *10*, 4117–4122.

(7) Willets, K. A.; Van Duyne, R. P. Localized Surface Plasmon Resonance Spectroscopy and Sensing. *Annu. Rev. Phys. Chem.* **2007**, *58*, 267–297.

(8) Kennedy, L. C.; Bickford, L. R.; Lewinski, N. A.; Coughlin, A. J.; Hu, Y.; Day, E. S.; West, J. L.; Drezek, R. A. A New Era for Cancer Treatment: Gold-Nanoparticle-Mediated Thermal Therapies. *Small* **2010**, *7*, 169–183.

(9) Sperling, R. A.; Rivera Gil, P.; Zhang, F.; Zanella, M.; Parak, W. J. Biological Applications of Gold Nanoparticles. *Chem. Soc. Rev.* **2008**, *37*, 1896–1908.

(10) Rosi, N. L.; Giljohann, D. A.; Thaxton, C. S.; Lytton-Jean, A. K. R.; Han, M. S.; Mirkin, C. A. Oligonucleotide-Modified Gold Nanoparticles for Intracellular Gene Regulation. *Science* **2006**, *312*, 1027–1030.

(11) Chen, J. I. L.; Chen, Y.; Ginger, D. S. Plasmonic Nanoparticle Dimers for Optical Sensing of DNA in Complex Media. *J. Am. Chem. Soc.* **2010**, *132*, 9600–9601.

(12) Jain, P. K.; Huang, X.; El-Sayed, I. H.; El-Sayed, M. A. Noble Metals on the Nanoscale: Optical and Photothermal Properties and Some Applications in Imaging, Sensing, Biology, and Medicine. *Acc. Chem. Res.* **2008**, *41*, 1578–1586.

(13) Mock, J. J.; Barbic, M.; Smith, D. R.; Schultz, D. A.; Schultz, S. Shape Effects in Plasmon Resonance of Individual Colloidal Silver Nanoparticles. *J. Chem. Phys.* **2002**, *116*, 6755–6759.

(14) Sonnichsen, C.; Franzl, T.; Wilk, T.; von Plessen, G.; Feldmann, J.; Wilson, O.; Mulvaney, P. Drastic Reduction of Plasmon Damping in Gold Nanorods. *Phys. Rev. Lett.* **2002**, *88*, 077402-1–077402-4.

(15) Chandra, M.; Dowgiallo, A.-M.; Knappenberger, K. L., Jr. Controlled Plasmon Resonance Properties of Hollow Gold Nanosphere Aggregates. *J. Am. Chem. Soc.* **2010**, *132*, 15782–15789.

(16) Nordlander, P.; Oubre, C.; Prodan, E.; Li, K.; Stockman, M. I. Plasmon Hybridization in Nanoparticle Dimers. *Nano Lett.* **2004**, *4*, 899–903.

(17) Pecharroman, C. Influence of the Close Sphere Interaction on the Surface Plasmon Resonance Absorption Peak. *Phys. Chem. Chem. Phys.* **2009**, *11*, 5922–5929.

(18) Brown, L. V.; Sobhani, H.; Lassiter, J. B.; Nordlander, P.; Halas, N. J. Heterodimers: Plasmonic Properties of Mismatched Nanoparticle Pairs. *ACS Nano* **2010**, *4*, 819–832.

(19) Chang, W.-S.; Slaughter, L. S.; Khanal, B. P.; Manna, P.; Zubarev, E. R.; Link, S. One-Dimensional Coupling of Gold Nanoparticle Plasmons in Self-Assembled Ring Superstructures. *Nano Lett.* **2009**, *9*, 1152–1157.

(20) Funston, A. M.; Novo, C.; Davis, T. J.; Mulvaney, P. Plasmon Coupling of Gold Nanorods at Short Distances and in Different Geometries. *Nano Lett.* **2009**, *9*, 1651–1658.

(21) Khlebtsov, B.; Zharov, V.; Melnikov, A.; Tuchin, V.; Khlebtsov, N. Optical Amplification of Photothermal Therapy with Gold Nanoparticles and Nanoclusters. *Nanotechnology* **2006**, *17*, 5167–5179.

(22) Kim, D.-S.; Heo, J.; Ahn, S.-H.; Han, S. W.; Yun, W. S.; Kim, Z. H. Real-Space Mapping of the Strongly Coupled Plasmons of Nanoparticle Dimers. *Nano Lett.* **2009**, *9*, 3619–3625.

(23) Slaughter, L. S.; Wu, Y.; Willingham, B. A.; Nordlander, P.; Link, S. Effects of Symmetry Breaking and Conductive Contact on the Plasmon Coupling in Gold Nanorod Dimers. *ACS Nano* **2010**, *4*, 4657–4666.

(24) Su, K. H.; Wei, Q. H.; Zhang, X.; Mock, J. J.; Smith, D. R.; Schultz, S. Interparticle Coupling Effects on Plasmon Resonances of Nanogold Particles. *Nano Lett.* **2003**, *3*, 1087–1090.

(25) Yang, L.; Wang, H.; Yan, B.; Reinhard, B. M. Calibration of Silver Plasmon Rulers in the 1−25 Nm Separation Range: Experimental Indications of Distinct Plasmon Coupling Regimes. *J. Phys. Chem. C* **2010**, *114*, 4901–4908.

(26) Willingham, B. A.; Brandl, D. W.; Nordlander, P. Plasmon Hybrization in Nanorod Dimers. *Appl. Phys. B: Lasers Opt.* **2008**, *93*, 209–216.

(27) Camden, J. P.; Dieringer, J. A.; Wang, Y.; Masiello, D. J.; Marks, L. D.; Schatz, G. C.; Van Duyne, R. P. Probing the Structure of Single-Molecule Surface-Enhanced Raman Scattering Hot Spots. *J. Am. Chem. Soc.* **2008**, *130*, 12616–12617.

(28) Kundu, J.; Le, F.; Nordlander, P.; Halas, N. J. Surface Enhanced Infrared Absorption (SEIRA) Spectroscopy on Nanoshell Aggregate Substrates. *Chem. Phys. Lett.* **2008**, *452*, 115–119.

(29) Rycenga, M.; Camargo, P. H. C.; Li, W.; Moran, C. H.; Xia, Y. Understanding the SERS Effects of Single Silver Nanoparticles and Their Dimers, One at a Time. *J. Phys. Chem. Lett.* **2010**, *1*, 696–703.

(30) Kinkhabwala, A.; Yu, Z.; Fan, S.; Avlasevich, Y.; Mullen, K.; Moerner, W. E. Large Single-Molecule Fluorescence Enhancements Produced by a Bowtie Nanoantenna. *Nat Photon* **2009**, *3*, 654–657.

(31) Kim, S.; Jin, J.; Kim, Y.-J.; Park, I.-Y.; Kim, Y.; Kim, S.-W. High-Harmonic Generation by Resonant Plasmon Field Enhancement. *Nature* **2008**, *453*, 757–760.

(32) Liu, M.; Lee, T.-W.; Gray, S. K.; Guyot-Sionnest, P.; Pelton, M. Excitation of Dark Plasmons in Metal Nanoparticles by a Localized Emitter. *Phys. Rev. Lett.* **2009**, *102*, 107401.

(33) Seol, Y.; Carpenter, A. E.; Perkins, T. T. Gold Nanoparticles: Enhanced Optical Trapping and Sensitivity Coupled with Significant Heating. *Opt. Lett.* **2006**, *31*, 2429–2431.

(34) Lassiter, J. B.; Aizpurua, J.; Hernandez, L. I.; Brandl, D. W.; Romero, I.; Lal, S.; Hafner, J. H.; Nordlander, P.; Halas, N. J. Close Encounters between Two Nanoshells. *Nano Lett.* **2008**, *8*, 1212–1218.

(35) Chen, H. J.; Sun, Z. H.; Ni, W. H.; Woo, K. C.; Lin, H. Q.; Sun, L. D.; Yan, C. H.; Wang, J. F. Plasmon Coupling in Clusters Composed of Two-Dimensionally Ordered Gold Nanocubes. *Small* **2009**, *5*, 2111–2119.

(36) Deutsch, B.; Hillenbrand, R.; Novotny, L. Visualizing the Optical Interaction Tensor of a Gold Nanoparticle Pair. *Nano Lett.* **2010**, *10*, 652–656.

(37) Maier, S. A.; Kik, P. G.; Atwater, H. A.; Meltzer, S.; Harel, E.; Koel, B. E.; Requicha, A. A. G. Local Detection of Electromagnetic Energy Transport Below the Diffraction Limit in Metal Nanoparticle Plasmon Waveguides. *Nat. Mater.* **2003**, *2*, 229–232.

(38) Willingham, B.; Link, S. Energy Transport in Metal Nanoparticle Chains Via Sub-Radiant Plasmon Modes. *Opt. Express* **2011**, *19*, 6450–6461.

(39) Citrin, D. S. Plasmon Polaritons in Finite-Length Metallic Nanoparticle Chains: The Role of Chain Length Unravelled. *Nano Lett.* **2005**, *5*, 985–989.

(40) Harris, N.; Arnold, M. D.; Blaber, M. G.; Ford, M. J. Plasmonic Resonances of Closely Coupled Gold Nanosphere Chains. *J. Phys. Chem. C* **2009**, *113*, 2784–2791.

(41) deWaele, R.; Koenderink, A. F.; Polman, A. Tunable Nanoscale Localization of Energy on Plasmon Particle Arrays. *Nano Lett.* **2007**, *7*, 2004–2008.

(42) Liu, K.; Nie, Z.; Zhao, N.; Li, W.; Rubinstein, M.; Kumacheva, E. Step-Growth Polymerization of Inorganic Nanoparticles. *Science* **2010**, *329*, 197–200.

(43) Murphy, C. J.; Thompson, L. B.; Alkilany, A. M.; Sisco, P. N.; Boulos, S. P.; Sivapalan, S. T.; Yang, J. A.; Chernak, D. J.; Huang, J. The Many Faces of Gold Nanorods. *J. Phys. Chem. Lett.* **2010**, *1*, 2867–2875.

(44) Wang, Y.; DePrince, A. E.; K. Gray, S.; Lin, X.-M.; Pelton, M. Solvent-Mediated End-to-End Assembly of Gold Nanorods. *J. Phys. Chem. Lett.* **2010**, *1*, 2692–2698.

(45) Nie, Z.; Fava, D.; Kumacheva, E.; Zou, S.; Walker, G. C.; Rubinstein, M. Self-Assembly of Metal-Polymer Analogues of Amphiphilic Triblock Copolymers. *Nat. Mater.* **2007**, *6*, 609–614.

(46) Khanal, B. P.; Zubarev, E. R. Rings of Nanorods. *Angew. Chem., Int. Ed.* **2007**, *46*, 2195–2198.

(47) Guffey, M. J.; Scherer, N. F. All-Optical Patterning of Au Nanoparticles on Surfaces Using Optical Traps. *Nano Lett.* **2010**, *10*, 4302–4308.

(48) Urban, A. S.; Lutich, A. A.; Stefani, F. D.; Feldmann, J. Laser Printing Single Gold Nanoparticles. *Nano Lett.* **2010**, *10*, 4794–4798.

(49) McMahon, J. M.; Wang, Y.; Sherry, L. J.; Van Duyne, R. P.; Marks, L. D.; Gray, S. K.; Schatz, G. C. Correlating the Structure, Optical Spectra, and Electrodynamics of Single Silver Nanocubes. *J. Phys. Chem. C* **2009**, *113*, 2731–2735.

(50) Knight, M. W.; Wu, Y.; Lassiter, J. B.; Nordlander, P.; Halas, N. J. Substrates Matter: Influence of an Adjacent Dielectric on an Individual Plasmonic Nanoparticle. *Nano Lett.* **2009**, *9*, 2188–2192.

(51) Hu, M.; Novo, C.; Funston, A.; Wang, H.; Staleva, H.; Zou, S.; Mulvaney, P.; Xia, Y.; Hartland, G. V. Dark-Field Microscopy Studies of Single Metal Nanoparticles: Understanding the Factors That Influence the Linewidth of the Localized Surface Plasmon Resonance. *J. Mater. Chem.* **2008**, *18*, 1949–1960.

(52) Slaughter, L. S.; Chang, W.-S.; Swanglap, P.; Tcherniak, A.; Khanal, B. P.; Zubarev, E. R.; Link, S. Single-Particle Spectroscopy of Gold Nanorods Beyond the Quasi-Static Limit: Varying the Width at Constant Aspect Ratio. *J. Phys. Chem. C* **2010**, *114*, 4934–4938.

(53) Boyer, D.; Tamarat, P.; Maali, A.; Lounis, B.; Orrit, M. Photothermal Imaging of Nanometer-Sized Metal Particles among Scatterers. *Science* **2002**, *297*, 1160–1163.

(54) Chang, W.-S.; Ha, J. W.; Slaughter, L. S.; Link, S. Plasmonic Nanorod Absorbers as Orientation Sensors. *Proc. Natl. Acad. Sci. U.S.A.* **2010**, *107*, 2781–2786.

(55) Sonnichsen, C.; Alivisatos, A. P. Gold Nanorods as Novel Nonbleaching Plasmon-Based Orientation Sensors for Polarized Single-Particle Microscopy. *Nano Lett.* **2005**, *5*, 301–304.

(56) Tcherniak, A.; Ha, J. W.; Dominguez-Medina, S.; Slaughter, L. S.; Link, S. Probing a Century Old Prediction One Plasmonic Particle at a Time. *Nano Lett.* **2010**, *10*, 1398–1404.

(57) Sönnichsen, C.; Franzl, T.; Wilk, T.; von Plessen, G.; Feldmann, J. Plasmon Resonances in Large Noble-Metal Clusters. *New J. Phys.* **2002**, *4*, 93.

(58) Berciaud, S.; Cognet, L.; Blab, G. A.; Lounis, B. Photothermal Heterodyne Imaging of Individual Nonfluorescent Nanoclusters and Nanocrystals. *Phys. Rev. Lett.* **2004**, *93*, 257402-1–257402-4.

(59) Gaiduk, A.; Ruijgrok, P. V.; Yorulmaz, M.; Orrit, M. Detection Limits in Photothermal Microscopy. *Chem. Sci.* **2010**, *1*, 343–350.

(60) Farrer, R. A.; Butterfield, F. L.; Chen, V. W.; Fourkas, J. T. Highly Efficient Multiphoton-Absorption-Induced Luminescence from Gold Nanoparticles. *Nano Lett.* **2005**, *5*, 1139–1142.

(61) Kreibig, U.; Vollmer, M. *Optical Properties of Metal Clusters*; Springer-Verlag: Berlin, 1995; Vol. 25.

(62) Schmucker, A. L.; Harris, N.; Banholzer, M. J.; Blaber, M. G.; Osberg, K. D.; Schatz, G. C.; Mirkin, C. A. Correlating Nanorod Structure with Experimentally Measured and Theoretically Predicted Surface Plasmon Resonance. *ACS Nano* **2010**, *4*, 5453–5463.

(63) Ming, T.; Zhao, L.; Yang, Z.; Chen, H.; Sun, L.; Wang, J.; Yan, C. Strong Polarization Dependence of Plasmon-Enhanced Fluorescence on Single Gold Nanorods. *Nano Lett.* **2009**, *9*, 3896–3903.

(64) Murphy, C. J.; Sau, T. K.; Gole, A. M.; Orendorff, C. J.; Gao, J.; Gou, L.; Hunyadi, S. E.; Li, T. Anisotropic Metal Nanoparticles: Synthesis, Assembly, and Optical Applications. *J. Phys. Chem. B* **2005**, *109*, 13857–13870.

(65) Marhaba, S.; Bachelier, G.; Bonnet, C.; Broyer, M.; Cottancin, E.; Grillet, N.; Lerme, J.; Vialle, J.-L.; Pellarin, M. Surface Plasmon Resonance of Single Gold Nanodimers near the Conductive Contact Limit. *J. Phys. Chem. C* **2009**, *113*, 4349–4356.

(66) Bryant, G. W.; Garcia de Abajo, F. J.; Aizpurua, J. Mapping the Plasmon Resonances of Metallic Nanoantennas. *Nano Lett.* **2008**, *8*, 631–636.

(67) Meier, M.; Wokaun, A. Enhanced Fields on Large Metal Paricles: Dynamic Depolarization. *Opt. Lett.* **1983**, *8*, 581–583.

(68) Kelly, K. L.; Coronado, E.; Zhao, L. L.; Schatz, G. C. The Optical Properties of Metal Nanoparticles: The Influence of Size, Shape, and Dielectric Environment. *J. Phys. Chem. B* **2002**, *107*, 668–677.
(69) Payne, E. K.; Shuford, K. L.; Park, S.; Schatz, G. C.; Mirkin, C. A. Multipole Plasmon Resonances in Gold Nanorods. *J. Phys. Chem. B* **2006**, *110*, 2150–2154.
(70) Heckel, J. C.; Chumanov, G. Depolarized Light Scattering from Single Silver Nanoparticles. *J. Phys. Chem. C* **2011**, *115*, 7261–7269.
(71) Kumbhar, A. S.; Kinnan, M. K.; Chumanov, G. Multipole Plasmon Resonances of Submicron Silver Particles. *J. Am. Chem. Soc.* **2005**, *127*, 12444–12445.
(72) Esteban, R.; Vogelgesang, R.; Dorfmüller, J.; Dmitriev, A.; Rockstuhl, C.; Etrich, C.; Kern, K. Direct Near-Field Optical Imaging of Higher Order Plasmonic Resonances. *Nano Lett.* **2008**, *8*, 3155–3159.
(73) Lee, J.; Hasan, W.; Lee, M. H.; Odom, T. W. Optical Properties and Magnetic Manipulation of Bimaterial Nanopyramids. *Adv. Mater.* **2007**, *19*, 4387–4391.
(74) Kinnan, M. K.; Chumanov, G. Plasmon Coupling in Two-Dimensional Arrays of Silver Nanoparticles: II. Effect of the Particle Size and Interparticle Distance. *J. Phys. Chem. C* **2010**, *114*, 7496–7501.
(75) Encina, E. R.; Coronado, E. A. Resonance Conditions for Multipole Plasmon Excitations in Noble Metal Nanorods. *J. Phys. Chem. C* **2007**, *111*, 16796–16801.
(76) Zuloaga, J.; Prodan, E.; Nordlander, P. Quantum Description of the Plasmon Resonances of a Nanoparticle Dimer. *Nano Lett.* **2009**, *9*, 887–891.
(77) Pramod, P.; Thomas, K. G. Plasmon Coupling in Dimers of Au Nanorods. *Adv. Mater.* **2008**, *20*, 4300–4305.
(78) Billaud, P.; Marhaba, S.; Cottancin, E.; Arnaud, L.; Bachelier, G.; Bonnet, C.; Del Fatti, N.; Lerme, J.; Vallee, F.; Vialle, J. L.; Broyer, M.; Pellarin, M. Correlation between the Extinction Spectrum of a Single Metal Nanoparticle and Its Electron Microscopy Image. *J. Phys. Chem. C* **2008**, *112*, 978–982.